Supplementary Information for

Engineering heterostructured nickel-cobalt sulfide@hydroxide nanoarrays with spontaneous and fast interfacial charge transfer for high-energy-density supercapacitors

Shensong Wang[a], Wuyou Jiang[a], Jintao Wu[a], Haitao Huang[b,*], Peng Guo[a], Xinyi Zhang[a,*], Haoshuang Gu[a], Qiu-an Huang[c], Yongming Hu[a,*]

[a] *Hubei Key Laboratory of Ferro- & Piezoelectric Materials and Devices, Faculty of Physics and Electronic Science, Hubei University, Wuhan 430062, China*

[b]*Department of Applied Physics, The Hong Kong Polytechnic University, Hong Kong, China*

[c] *Institute for Sustainable Energy/College of Sciences, Shanghai University, Shanghai 200444, P.R. China*

***Corresponding authors**

E-mail: aphhuang@polyu.edu.hk (Haitao Huang), xinyizhang@hubu.edu.cn (Xinyi Zhang), huym@hubu.edu.cn (Yongming Hu)

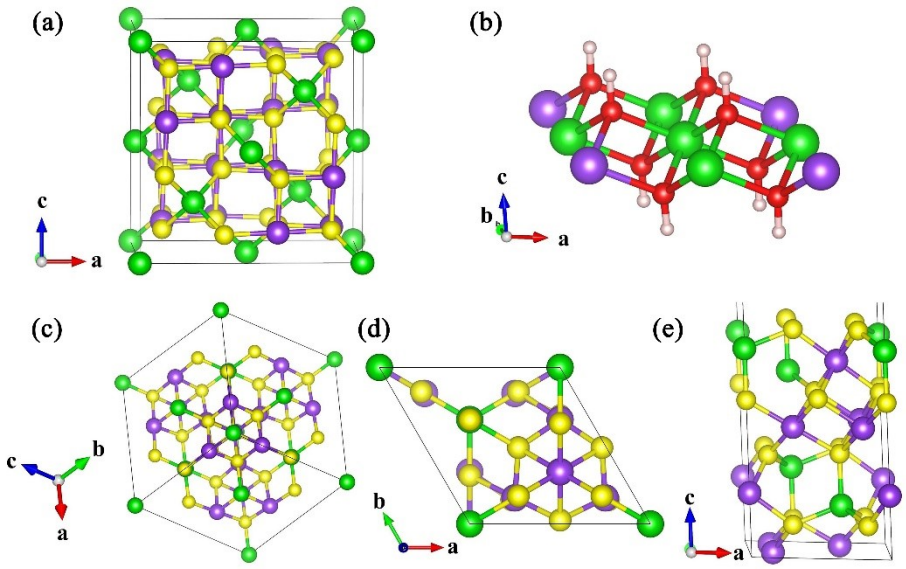

Figure S1. The atomic structure of models. (a) $NiCo_2S_4$. (b) Ni_3-Co LDH. (c) Visual angle of the $NiCo_2S_4$ (1 1 1) surface. (d, e) $NiCo_2S_4$ (1 1 1) section surface models (Co: purple atom, S: yellow atom, Ni: green atom, O: red atom and H: white atom).

Figure S1a and **S1b** is the atomic structure of $NiCo_2S_4$ and Ni-Co LDH (0 0 1) surface, where $NiCo_2S_4$ belongs to cubic system and Ni-Co LDH belongs to hexagonal system. In order to build a reasonable heterojunction model, it need to find matching crystal planes. **Figure S1c** is the visual angle of the $NiCo_2S_4$ (1 1 1) surface. It can be seen that the crystals exhibit a typical regular hexagonal structure. Therefore, we sliced the $NiCo_2S_4$ crystal from the (1 1 1) crystal plane and the cleaving thickness is 2. The structures are shows in **Figure S1d** and **S1e**. The lattice constants "a" of $NiCo_2S_4$ (1 1 1) and Ni-Co LDH (0 0 1) are 6.594 Å and 6.316 Å, which satisfies the condition that the lattice mismatch rate is less than 5%.

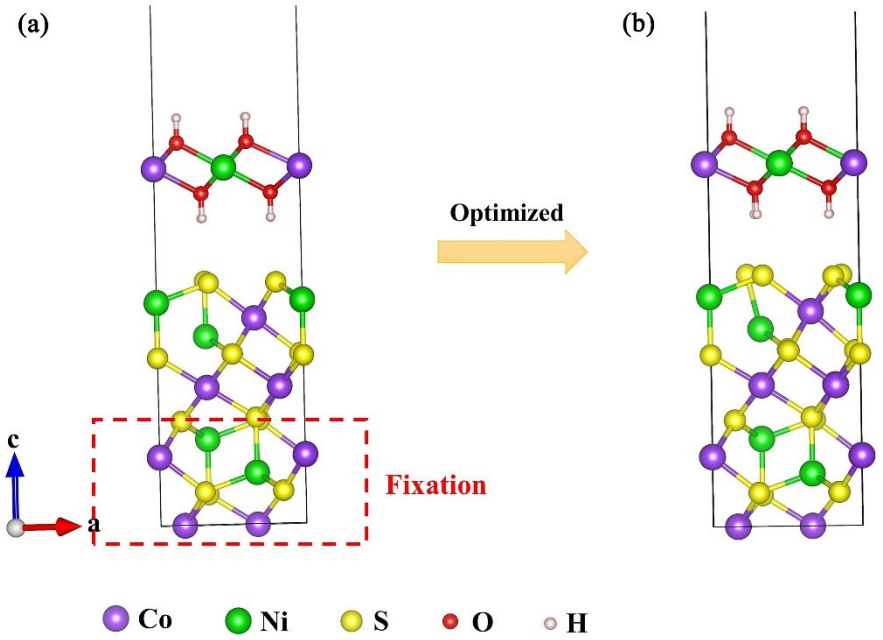

Figure S2. The initial model (a) and optimized result (b) of the NCS@NC LDH heterojunction.

Figure S2a is the initial model of NCS@NC LDH heterojunction (lattice constants: a = b = 6.594 Å, c = 31 Å). Considering that the heterojunction constructed by van der Waals adsorption mainly affects the atoms on the surface or near surface, we fixed some atoms to keep their relative positions unchanged during structure optimization, which was marked by the red rectangle area. **Figure S2b** is the optimized result (lattice constants: a = 6.585 Å, b = 6.584 Å, c = 31 Å). It can be seen the S atoms on the top have undergone a significant shift, which means that there is a charge interaction between $NiCo_2S_4$ and Ni-Co LDH.

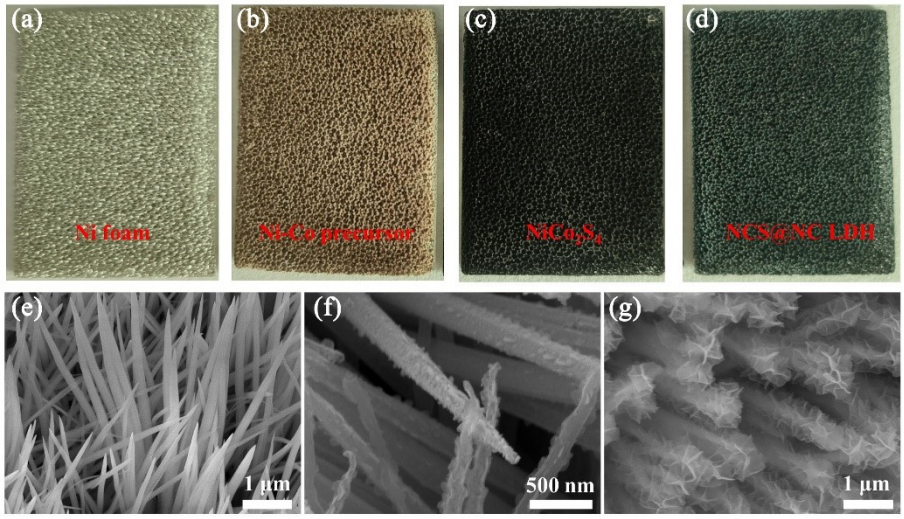

Figure S3. (a-d) The photograph of as-prepared samples. High magnification SEM images of (e) Ni-Co precursor, (f) $NiCo_2S_4$ and (g) NCS@NC LDH.

Figures S3a-d is the photograph of as-prepared samples. The color of pure Ni foam, Ni-Co precursor, $NiCo_2S_4$ and $NiCo_2S_4$@Ni-Co LDH are silvery white, pink, black and jasper, respectively. **Figure S3e** is the SEM image of Ni-Co precursor nanotubes. It can be seen their surfaces are smooth, while the $NiCo_2S_4$ nanotubes become rougher (**Figure S3f**). **Figure S3g** clearly shows that the Ni-Co LDH nanosheets are grown on the surface of $NiCo_2S_4$ nanotubes.

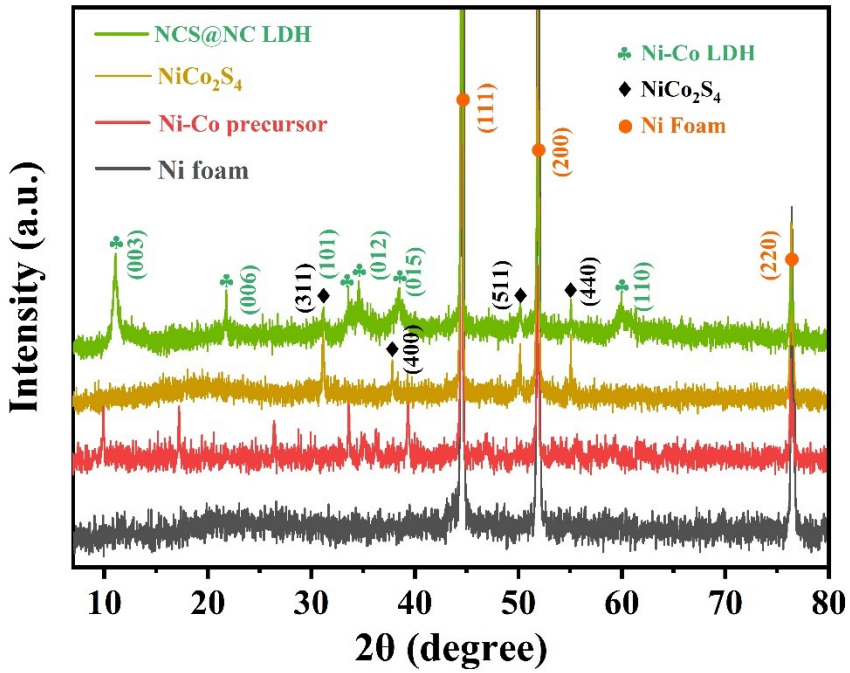

Figure S4. XRD patterns of the different samples.

As shown in **Figure S4**, the peaks located at 44.5°, 51.9° and 76.4° correspond to (1 1 1), (2 0 0) and (2 2 0) of Ni foam (JCPDS card no. 040850).[1] With the growth of $NiCo_2(CO_3)_x(OH)_{6-2x}$, some new peaks appear in the XRD pattern except Ni characteristic peaks. After sulfuration, all of the characteristic peaks of Ni-Co precursor are disappeared and transformed into $NiCo_2S_4$. The peaks located at 31.1°, 37.9o, 50.2, and 55.1° correspond to (3 1 1), (400), (511) and (440) of $NiCo_2S_4$ (JCPDS card no. 431477).[2] Finally, with the growth of Ni-Co LDH nanosheets, the (0 0 3), (006), (101), (012), (015) and (110) characteristic peaks of Ni-Co LDH appears,[3] while the characteristic peaks of $NiCo_2S_4$ and Ni foam still existed, which means that the composite of NCS@NC LDH are synthesized successfully.

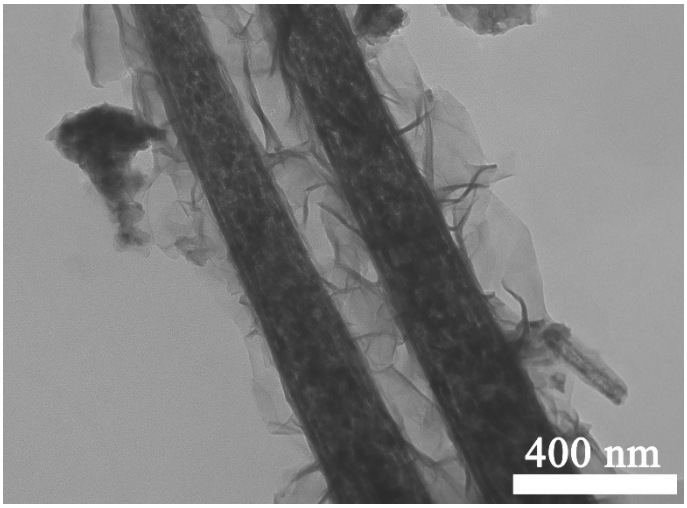

Figure S5. The TEM image of NCS@NC LDH.

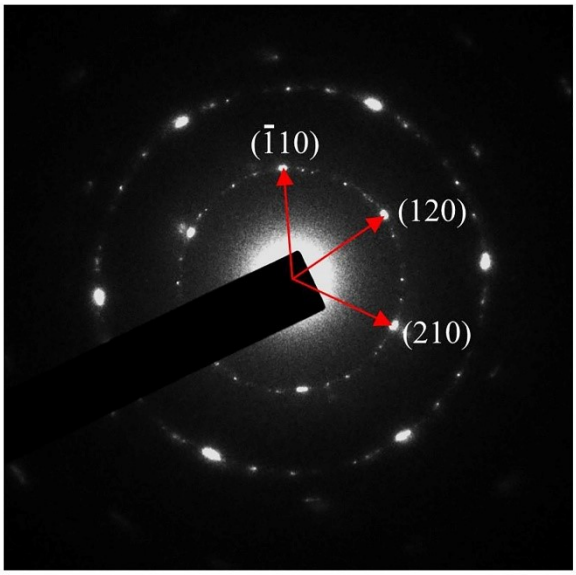

Figure S6. SAED image of Ni-Co LDH nanosheet from [001] zone axis.

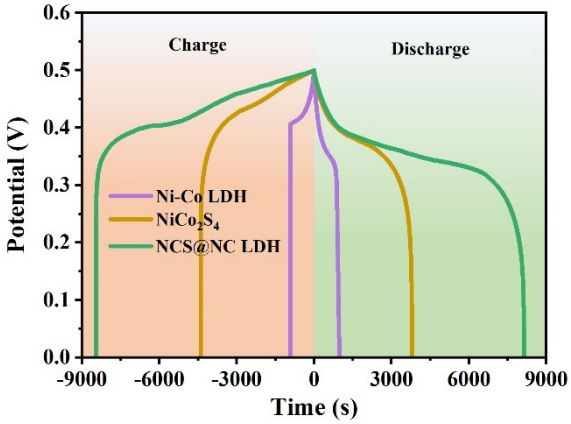

Figure S7. The comparative GCD curves of $NiCo_2S_4$ nanotubes, Ni-Co LDH nanosheets and NCS@NC LDH (2h) electrodes at 1 mA cm^{-2}.

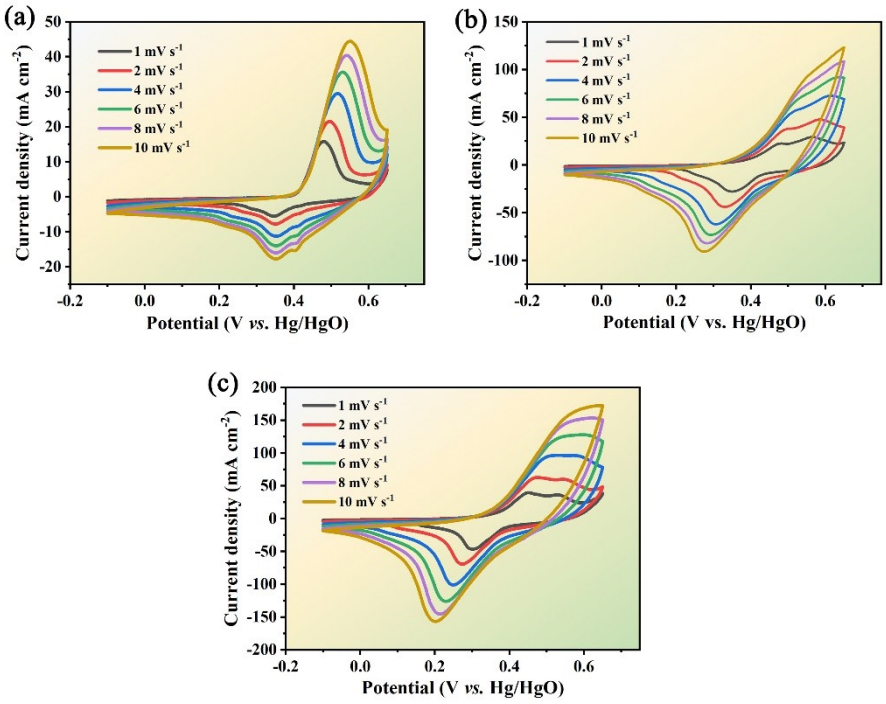

Figure S8. CV curves with scan rates from 1 mV s^{-1} to 10 mV s^{-1}. (a) Ni-Co LDH. (b) $NiCo_2S_4$. (c) NCS@NC LDH.

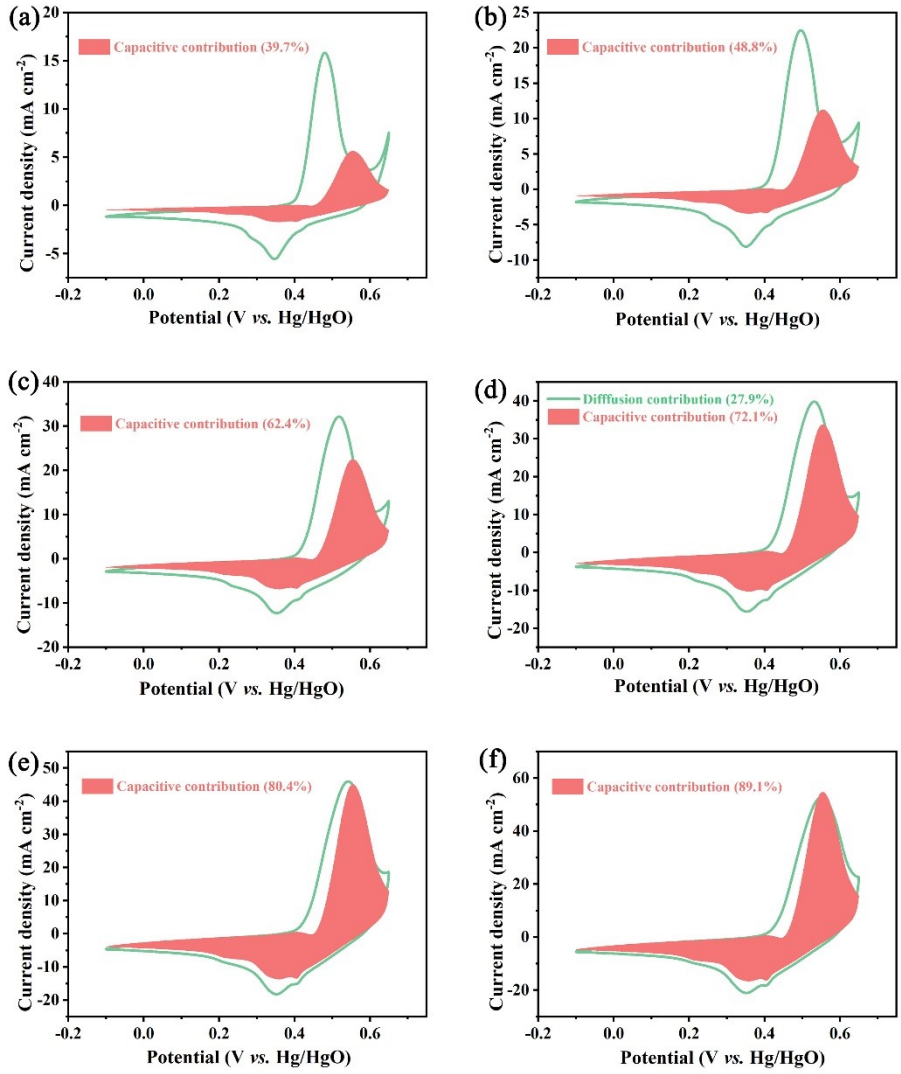

Figure S9. The diffusion contribution and capacitive contribution of Ni-Co LDH at different scan rates. (a) 1 mV s^{-1}. (b) 2 mV s^{-1}. (c) 4 mV s^{-1}. (d) 6 mV s^{-1}. (e) 8 mV s^{-1}. (f) 10 mV s^{-1}.

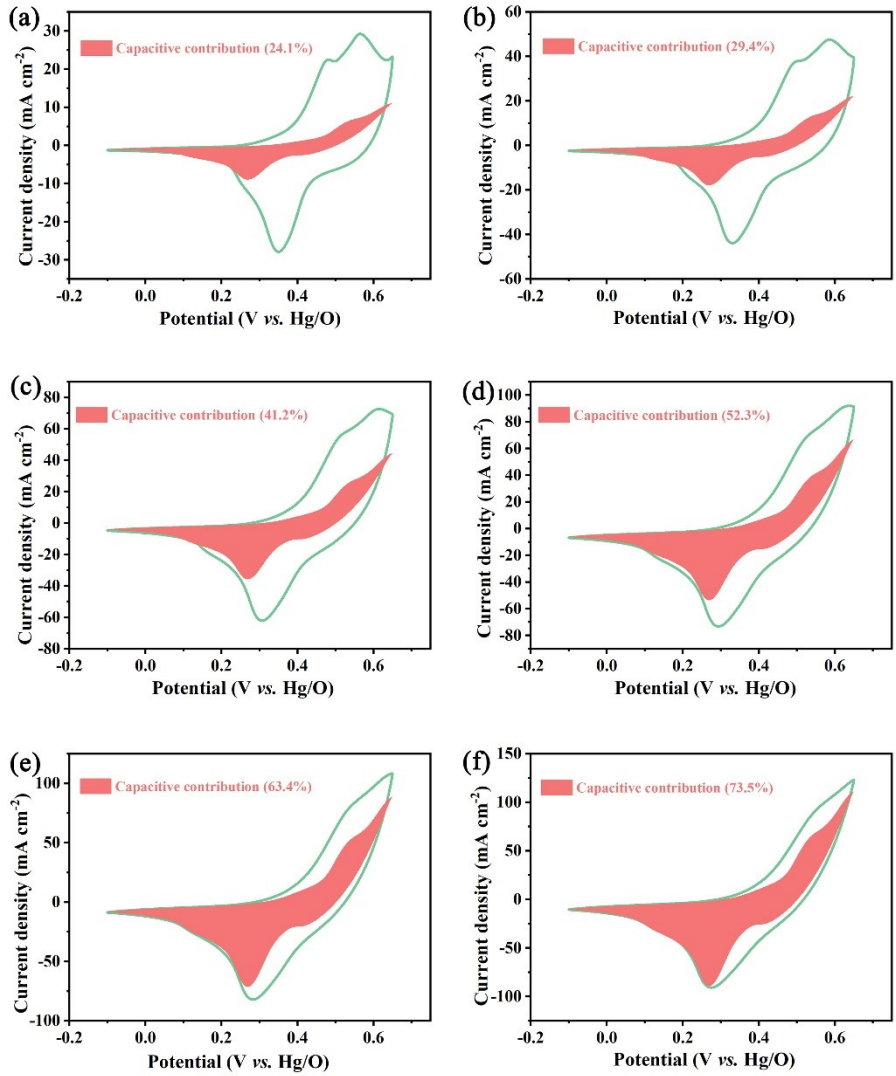

Figure S10. The diffusion contribution and capacitive contribution of $NiCo_2S_4$ at different scan rates. (a) 1 mV s^{-1}. (b) 2 mV s^{-1}. (c) 4 mV s^{-1}. (d) 6 mV s^{-1}. (e) 8 mV s^{-1}. (f) 10 mV s^{-1}.

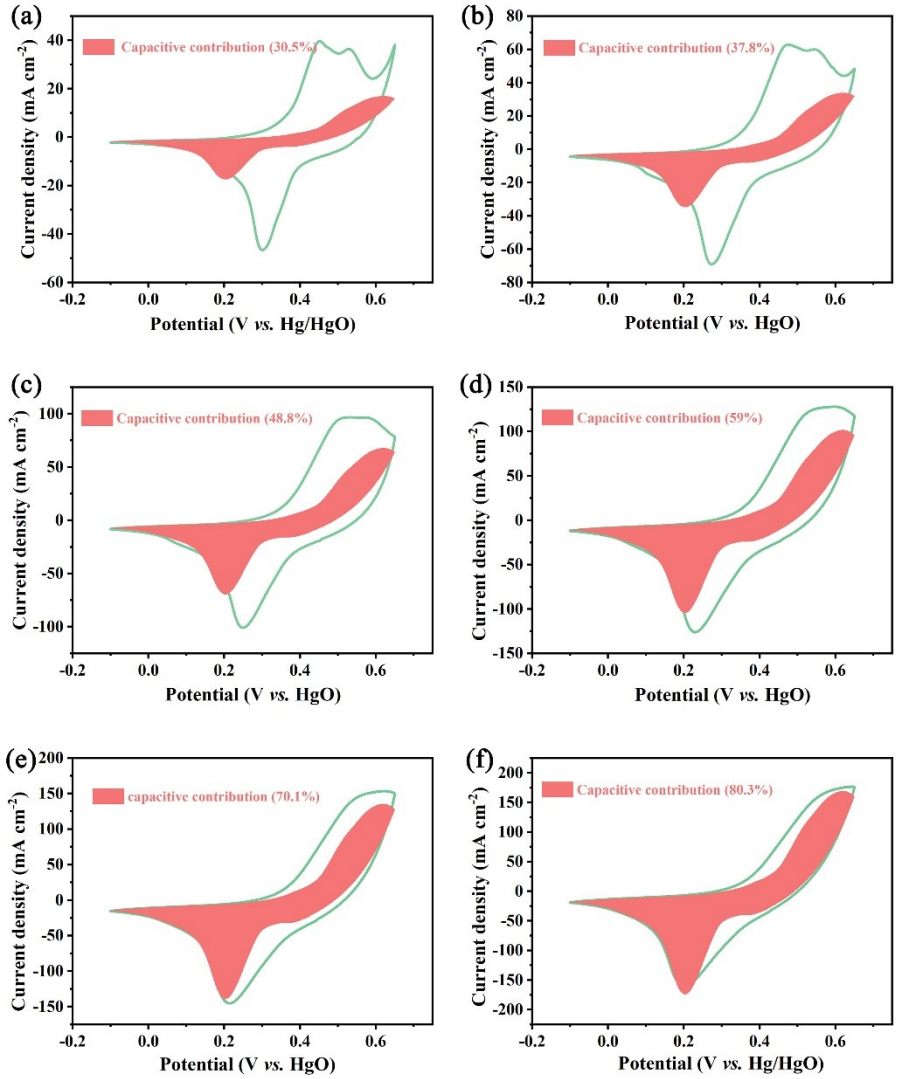

Figure S11. The diffusion contribution and capacitive contribution of NCS@NC LDH at different scan rates. (a) 1 mV s^{-1}. (b) 2 mV s^{-1}. (c) 4 mV s^{-1}. (d) 6 mV s^{-1}. (e) 8 mV s^{-1}. (f) 10 mV s^{-1}.

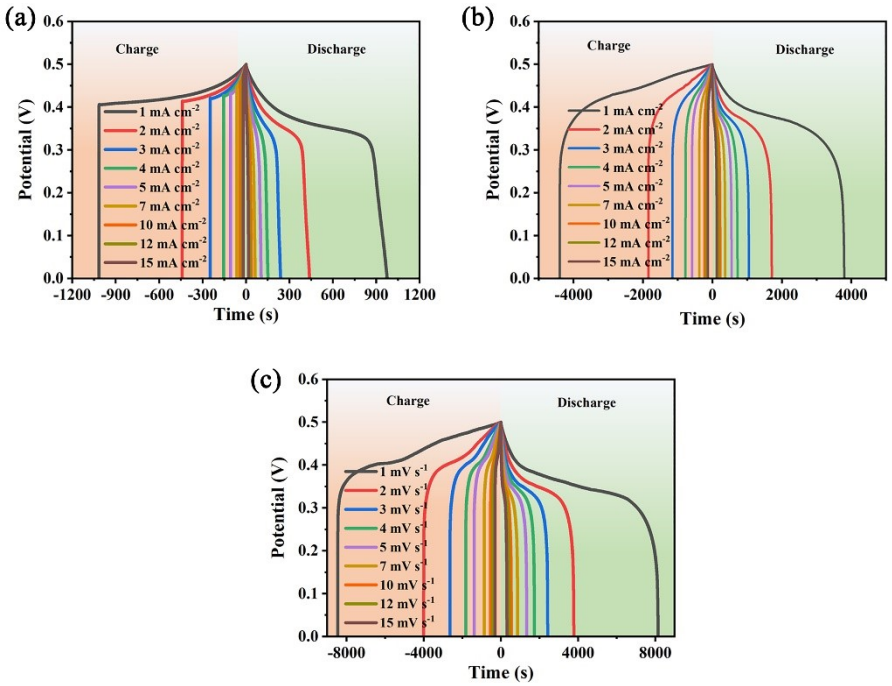

Figure S12. GCD curves with current density from 1 mA cm^{-2} to 15mA cm^{-2}. (a) Ni-Co LDH. (b) $NiCo_2S_4$. (c) NCS@NC LDH.

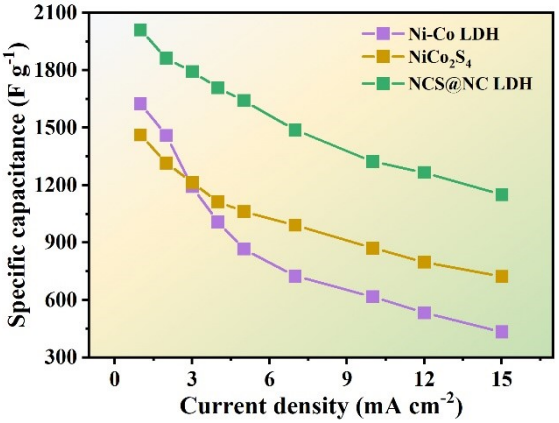

Figure S13. The specific capacitance of Ni-Co LDH, $NiCo_2S_4$ and NCS@NC LDH with current densities ranging from 1 mA cm^{-2} to 15 mA cm^{-2}.

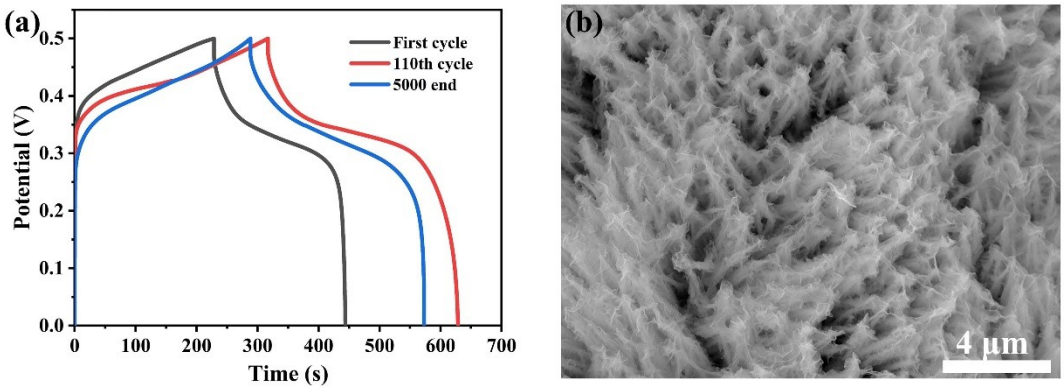

Figure S14. (a) The GCD curves of NCS@NC LDH electrode after 1 st, 110th and 5000th cycles at current density of 15 mA cm^{-2}. (b) The SEM image of NCS@NC LDH electrode after 5000 cycles.

Table S1

Comparison of core-shell structured electrode materials based on Ni-Co LDH in recent five years

Electrode materials	Mass loading	Specific capacitance	Current density	Stability (cycles)	Ref.
Co_9S_8@PPy@Ni-Co LDH	-	2.65 F cm^{-2}	1 mA cm^{-2}	88.67% (10000)	[4]
NiCoP@Ni-Co LDH	2.4 mg cm^{-2}	4.68 F cm^{-2}	1mA cm^{-2}	81.1% (5000)	[5]
Graphene@Ni-Co LDH	1.5 mg cm^{-2}	2.2 F cm^{-2}	1 A g^{-1}	81.6% (1000)	[6]
$CuCo_2S_4$@Ni-Co LDH	1.8 mg cm^{-2}	4.21 F cm^{-2}	1 A g^{-1}	59.2% (2000)	[7]
Zn-Ni-Co@Ni-Co LDH	2.3 mg cm^{-2}	6.59 F cm^{-2}	1 A g^{-1}	89% (8000)	[8]
$FeCo_2O_4$@Ni-Co LDH	5 mg cm^{-2}	12.13 F cm^{-2}	1 A g^{-1}	91.6% (5000)	[9]
Co_3O_4@Ni-Co LDH	4.5 mg cm^{-2}	12.05 F cm^{-2}	0.5 A g^{-1}	67.7% (10000)	[10]
$CoMoO_4$@Ni-Co LDH	3.2 mg cm^{-2}	6.48 F cm^{-2}	1 A g^{-1}	90.8% (5000)	[11]
Mo-NiS_2@Ni-Co LDH	2.35 mg cm^{-2}	6.12 F cm^{-2}	1 A g^{-1}	50.3% (3000)	[12]
MoO_{3-x}@Ni-Co LDH	-	3.49 F cm^{-2}	5 mA cm^{-2}	94.9% (3000)	[13]
CCCH@Ni-Co LDH	1.6 mg cm^{-2}	1.9 F cm^{-2}	10.6 mA cm^{-2}	90.8% (30000)	[14]
NCS@NC LDH	**8.1 mg cm^{-2}**	**16.28 F cm^{-2}**	**1 mA cm^{-2}**	**91.5% (5000)**	**This work**

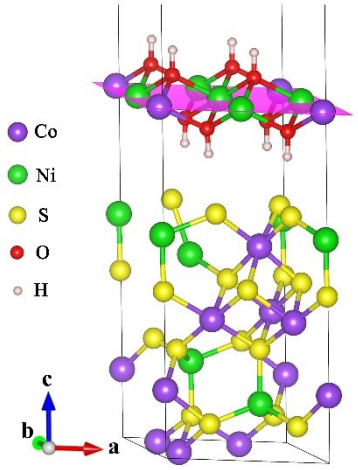

Figure S15. The structure model of NCS@NC LDH. The magenta area is the plane of local charge density.

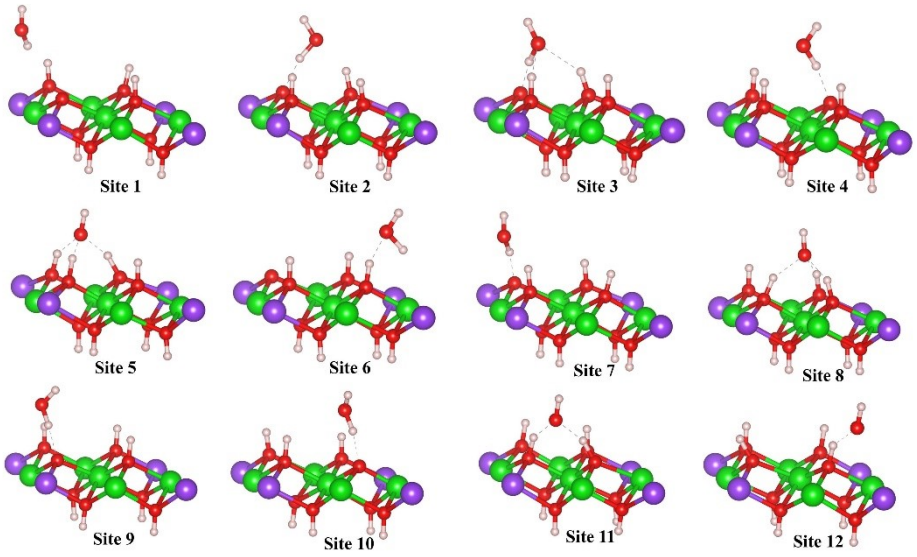

Figure S16. Optimized structural models after OH^- adsorption at different sites in pure Ni-Co LDH.

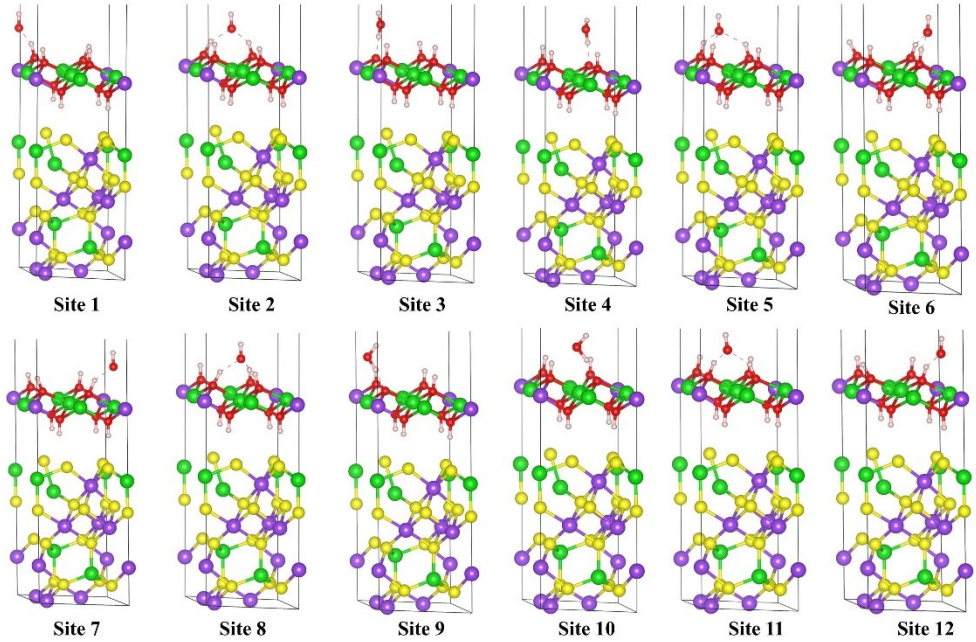

Figure S17. Optimized structural models after OH adsorption at different sites in pure Ni-Co LDH.

Table S2 The absorption energy of OH^- in pure Ni-Co LDH and NCS@NC LDH at different sites.

Structures	absorption energy of OH^- at different sites (eV)											
	1	2	3	4	5	6	7	8	9	10	11	12
Ni-Co LDH	**-1.451**	**-1.423**	**-1.398**	**-1.362**	**-1.355**	**-1.425**	**-1.423**	**-1.091**	**-1.400**	**-1.264**	**-1.237**	**-1.301**
NCS@NC LDH	**-1.378**	**-1.410**	**-1.873**	**-1.879**	**-1.143**	**-1.587**	**-1.311**	**-1.473**	**-1.503**	**-1.874**	**-1.596**	**-1.598**

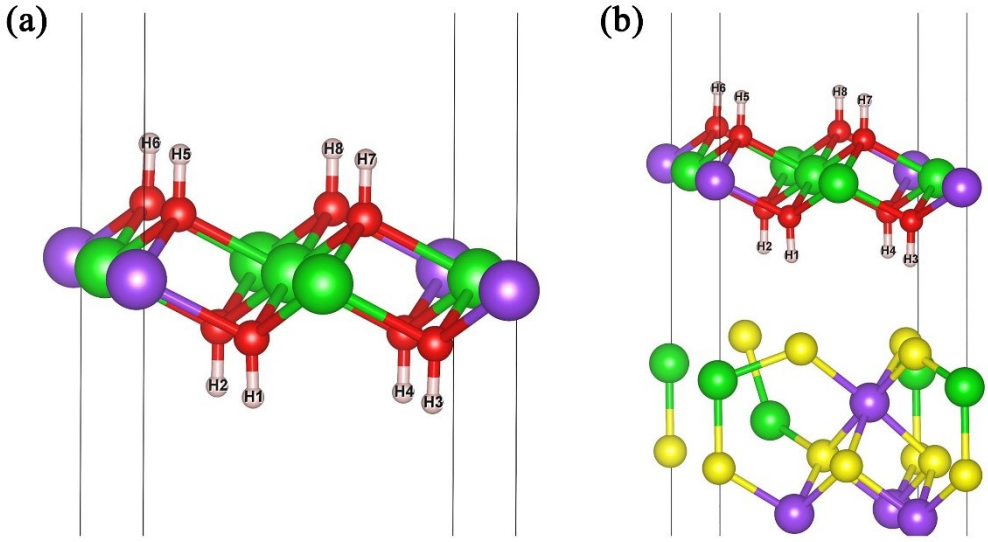

Figure S18. H desorption sites. (a) Ni-Co LDH. (b) NCS@NC LDH.

Table S3 The desorption energy of H in pure Ni-Co LDH and NCS@NC LDH

Structures	Desorption energy of H (eV)							
	H1	H2	H3	H4	H5	H6	H7	H8
Ni-Co LDH	**4.725**	**4.898**	**4.827**	**4.726**	**4.738**	**4.833**	**4.906**	**4.739**
NCS@NC LDH	**4.585**	**4.691**	**5.482**	**4.783**	**5.136**	**5.164**	**4.639**	**5.133**

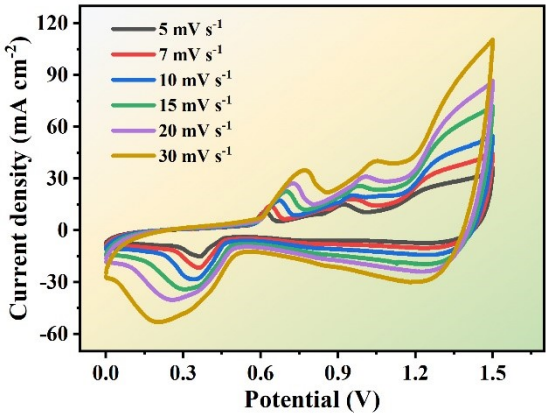

Figure S19. CV curves of the ASC at various scan rates.

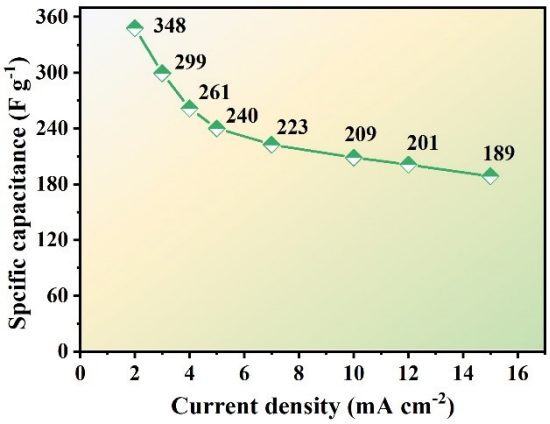

Figure S20. Specific capacitance of the ASC device at various current density.

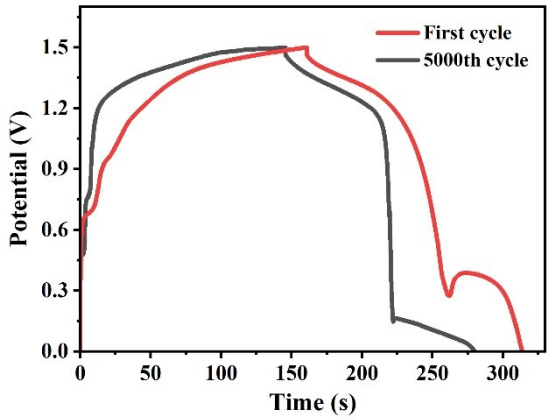

Figure S21. The GCD curves of ASC at first cycle and 5000th cycle under current density of 15 mA cm^{-2}.

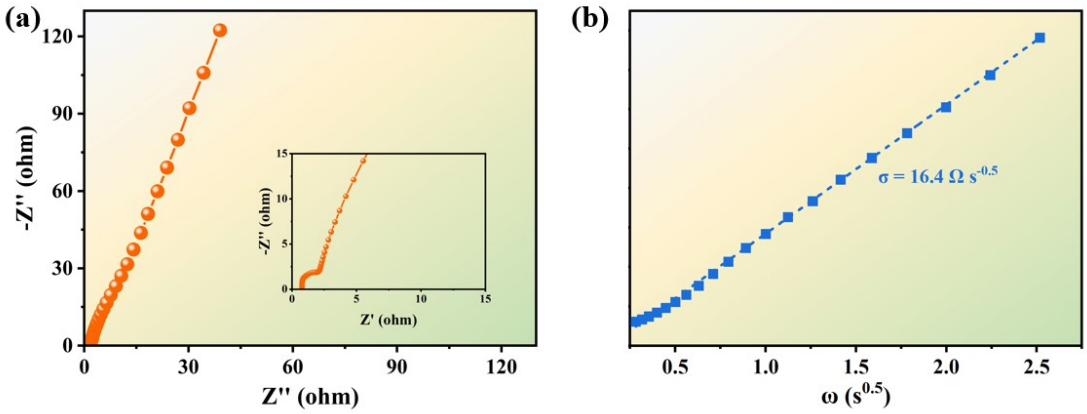

Figure S22. (a) The EIS of ASC. Insert is the part of high frequency region. (b) Randles plot of Z' vs $\omega^{-0.5}$.

Reference

1. S. Kim, J. Kang, S. Kim, J. Jang, *Nano Energy*, 2017, **39**, 639-646.

2. H. Chen, J. Jiang, L. Zhang, D. Xia, Y. Zhao, D. Guo, T. Qi, H. Wan, *J. Power Sources*, 2014, **254**, 249-257.

3. X. Bai, Q. Liu, H. Zhang, J. Liu, Z. Li, X. Jing, Y. Yuan, L. Liu, J. Wang, *Electrochim. Acta*, 2016, **215**, 492-499.

4. L. Wang, S. Li, F. Huang, X. Yu, M. Liu, H. Zhang, *J. Power Sources*, 2019, **439**, 227103.

5. X. Gao, Y. Zhao, K. Dai, J. Wang, B. Zhang, X. Shen, *Chem. Eng. J.*, 2020, **384**, 123373..

6. H. Kuang, H. Zhang, X. Liu, Y. Chen, W. Zhang, H. Chen, Q. Ling, *Carbon*, 2022, 190, 57-67.

7. P. Naveenkumar, G. Kalaignan, *Compos. Part B-Eng.*, 2019, **173**, 106864.

8. J. Acharya, T. Ko, M. Seo, M. Khil, H. Kim, B. Kim, *ACS Applied Energy Mater.*, 2020, **3**, 7383-7396.

9. X. He, R. Li, J. Liu, Q. Liu, R. Chen, D. Song, J. Wang, *Chem. Eng. J.*, 2018, **334**, 1573-1583.

10. J. Zhou, Q. Li, C. Chen, Y. Li, K. Tao, L. Han, *Chem. Eng. J.*, 2018, **350**, 551-558.

11. Y. Zhao, X. He, R. Chen, Q. Liu, J. Liu, J. Yu, J. Li, H. Zhang, H. Dong, M. Zhang, J. Wang, *Chem. Eng. J.*, 2018, **352**, 29-38.

12. M. Shi, M. Zhao, L. Jiao, Z. Su, M. Li, X. Song, *J. Power Sources*, 2021, **509**, 230333.

13. H. Zhang, Y. Lv, X. Wu, J. Guo, D. Jia, *Chem. Eng. J.*, 2022, **431**, 133233.

14. Y. Guo, X. Hong, Y. Wang, Q. Li, J. Meng, R. Dai, X. Liu, L. He, L. Mai, *Adv. Funct. Mater.*, 2019, **29**, 1809004.